

Geometric Evolution Graph Convolutional Networks: Enhancing Graph Representation Learning via Ricci Flow

Jicheng Ma¹, Yunyan Yang¹, Juan Zhao¹, and Liang Zhao^{2*}

¹School of Mathematics, Renmin University of China, Beijing, China.

²School of Mathematical Sciences, Key Laboratory of Mathematics and Complex Systems of MOE, Beijing Normal University, Beijing, China.

*Corresponding author: liangzhao@bnu.edu.cn

Abstract

We introduce the Geometric Evolution Graph Convolutional Network (GEGCN), a novel framework that enhances graph representation learning through explicit modeling of geometric evolution on graph structures. Specifically, GEGCN leverages a Long Short-Term Memory (LSTM) network to capture the dynamic structural sequence generated by discrete Ricci flow, and infuses the learned dynamic representations into a graph convolutional network. Extensive experiments demonstrate that GEGCN achieves excellent performance on classification tasks across various benchmark datasets, including homophilic/heterophilic graphs, filtered graphs, and large-scale graphs.

Keywords: Ricci Flow, Graph Convolutional Network, LSTM, Graph Representation Learning.

1 Introduction

Graph Neural Networks (GNNs), especially Graph Convolutional Networks (GCNs) and their variants, have achieved remarkable success for learning representations on graph-structured data, by iteratively propagating and aggregating information from a node’s local neighborhood [1]. Despite their effectiveness, most existing GNNs, such as GCN [2], GAT [3], and GraphSAGE [4], treat graphs as static snapshots, and focus on local message passing. This paradigm often overlooks the rich, global geometric properties inherent in graph structures.

Recently, the concept of discrete curvature [5–7] has been successfully adapted to network analysis. An expanding corpus of research confirms its utility as a principled way to characterize

local and global structural features of graphs, such as bottlenecks [8], community structure [9, 10], and network fragility [11]. This geometric perspective has naturally inspired notable efforts to integrate discrete curvature into GNN pipelines [8, 12, 13]. A critical observation, however, is that these methods rely on static, pre-computed curvature, thereby capturing only a single snapshot of graph geometry.

Discrete Ricci flow [5, 14–16], which deforms a metric space by iteratively redistributing curvature, offers a natural mechanism for modeling graph evolution, promising a deep, multi-scale understanding of graph structure [10, 17, 18]. Despite the theoretical appeal and structural utility of Ricci flow, a natural question remains rarely explored: how to systematically integrate Ricci flow into GNNs to learn more powerful

node representations.

In parallel, recurrent neural networks (RNNs), especially Long Short-Term Memory (LSTM) networks [19], have demonstrated strong capability in modeling temporal dependencies and structured sequences. Their effectiveness in capturing long-range dependence makes them suitable for learning from sequential data generated by dynamic systems. This makes them a particularly promising candidate for modeling the sequential graph structure generated by discrete Ricci flow, which is a natural dynamic process.

Motivated by these observations, we propose the Geometric Evolution Graph Convolutional Network (GEGCN), a novel framework that integrates Ricci flow with deep graph models by explicitly modeling geometric evolution as a sequential process. Specifically, we generate a sequence of evolving graphs via discrete Ricci flow, where each step reveals structural information at a different scale, and employ an LSTM to capture the structural dynamics. The learned multi-scale structural information is then incorporated into a GCN to enhance node embeddings for downstream tasks. In this way, GEGCN bridges discrete differential geometry and graph neural networks through a dynamic representation learning paradigm.

Extensive experiments demonstrate that GEGCN achieves state-of-the-art results on most benchmark datasets for node classification, with only slight performance drops on a small number of cases, demonstrating its overall superior performance. Further analysis shows that GEGCN better captures structural heterophily than existing baselines, leading to more effective and structurally informative node representations. These results highlight the importance of modeling geometric dynamics for graph learning and suggest a promising direction for unifying geometric analysis and graph neural networks.

Our contributions are summarized as follows:

(i) A New Geometric Perspective. We introduce discrete Ricci flow into deep graph

representation learning, providing a principled method to model the geometric evolution of graph structures.

(ii) A Simple Architecture. In contrast to methods relying on complex architectures for performance, the proposed GEGCN maintains a concise and elegant design by integrating Ricci flow, LSTM and GCN into a cohesive model. The highly competitive performance demonstrates that simplicity and effectiveness can coexist in graph neural networks.

(iii) Empirical Superiority. Extensive experiments across various scales, homophilic/heterophilic settings, and filtered benchmarks demonstrate that GEGCN achieves excellent performance, underscoring the critical value of geometric evolution for graph representation learning.

2 Related Works

Our work lies at the intersection of geometry of graphs, neural differential equations, and graph neural networks. We categorize related research into two primary strands, highlighting their distinctions from our proposed GEGCN.

2.1 Geometric Graph Neural Networks

A significant line of research enhances GNNs by incorporating discrete curvature or related metrics to modulate message passing. For instance, CurvGN [12] and CGNN [20] explicitly use Ollivier-Ricci curvature to reweight message passing, demonstrating improved performance. κ HGCN [21] utilizes a curvature-aware hyperbolic graph convolutional neural network in order to guide message passing of tree-like structures. SelfRGNN [22] tackles temporal graphs by formulating a time-dependent functional curvature to reweight message passing. RC-UFG [23] introduces two curvature-based framelet models, namely RC-UFG (Hom)

and RC-UFG (Het), showcasing their enhanced adaptability on homophilic and heterophilic graph datasets.

It is worth noting that Topping et al. [8] formally established the connection between oversquashing phenomena in GNNs and graph curvature. SDRF proposed in [8] is a curvature-based rewiring method that modifies graph topology, which the authors themselves note is “different from more direct extensions of Ricci flow on graphs”. Works [24, 25] follow a similar intent to [8] in their use of curvature. In this direction, CurvDrop [13] introduces a curvature-based dropout sampling technique to mitigate over-smoothing and oversquashing. CurvGIB [26] advances this by applying a variational information bottleneck principle, aiming to learn optimal information transport patterns for better node representations.

2.2 Neural Diffusion Equations on Graphs

Another category frames deep learning on graphs as diffusion processes. GRAND [27] and Beltrami flow [28] model feature propagation with diffusion equations, providing a principled, continuous-depth perspective on GNNs. Specifically, Beltrami flow employs the Laplace-Beltrami operator within a diffusion partial differential equation (PDE), making it a non-Euclidean diffusion process where node features are augmented with topology-derived positional encodings.

Closely related is GNRF [29], which conceptualizes node feature learning as a curvature-driven diffusion. GNRF essentially implements a learned, curvature-informed diffusion PDE rather than an explicit discrete Ricci flow that evolves the graph structure itself to generate a geometric sequence.

2.3 Summary and Positioning

Using curvature to guide message passing in GNNs has emerged as a well-recognized and natural idea in recent years. While existing geometric GNNs have validated the utility of curvature for enhancing model performance, GEGCN is a concise, principled design that differs from existing curvature-based approaches.

Existing works that incorporate curvature into GNNs typically rely on a static snapshot of curvature, whether pre-computed or learned as a fixed parameter. This captures only a single-scale geometric view and fails to model the intrinsic multi-scale evolution of graph structure. In contrast, our work introduces discrete Ricci flow as a dynamic structure generator, rooted in the geometric analysis framework originally extended to metric spaces by Ollivier [5].

While PDE-based diffusion models are powerful, they typically do not incorporate the geometric evolution enabled by discretized Ricci flow. In GNRF, curvature is predicted by an auxiliary neural module (EdgeNet). As the authors of GNRF note, EdgeNet can be viewed as approximating Ollivier-Ricci, Forman-Ricci, or other curvature forms. But the ultimate output of EdgeNet remains unclear, leaving open the question of whether it truly leverages the geometric meaning of curvature, though EdgeNet may still be useful for model performance. Our GEGCN evolves graph geometry via discrete Ollivier-Ricci flow and integrates the resulting dynamic geometric information into a standard GCN using an LSTM encoder, thereby capturing the full trajectory of geometric change.

3 Preliminaries

This section introduces the foundational concepts for our work. We first establish key notations and review the basics of graph neural networks. We then present the notions of discrete Ricci curvature and Ricci flow on graphs.

Finally, we discuss RNNs and the LSTM architecture.

3.1 Notations and Graph Convolutional Networks

Let $\mathcal{G} = (\mathcal{V}, \mathcal{E})$ denote an undirected graph, where $\mathcal{V} = \{v_1, \dots, v_N\}$ is the set of N nodes and $\mathcal{E} \subseteq \mathcal{V} \times \mathcal{V}$ is the set of edges. The graph structure is represented by an adjacency matrix $\mathbf{A} \in \{0, 1\}^{N \times N}$, where $\mathbf{A}_{ij} = 1$ if $(v_i, v_j) \in \mathcal{E}$ and 0 otherwise. Each node v_i is associated with a feature vector $\mathbf{x}_i \in \mathbb{R}^d$, and the node feature matrix is denoted as $\mathbf{X} \in \mathbb{R}^{N \times d}$. The neighborhood of node v_i is defined as $\mathcal{N}(i) = \{v_j \in \mathcal{V} : (v_i, v_j) \in \mathcal{E}\}$. The degree of v_i is $d_i = |\mathcal{N}(i)|$, and the degree matrix is $\mathbf{D} = \text{diag}(d_1, \dots, d_N)$.

Graph neural networks learn node representations by iteratively aggregating information from local neighborhoods, a paradigm known as message passing. As a foundational and widely adopted instance, the graph convolutional network layer implements a specific form of this mechanism. The layer-wise propagation rule of a GCN is defined as

$$\mathbf{H}^{(\ell+1)} = \sigma(\hat{\mathbf{A}}\mathbf{H}^{(\ell)}\mathbf{W}^{(\ell)}), \quad (1)$$

where $\mathbf{H}^{(\ell)} \in \mathbb{R}^{N \times h_\ell}$ is the matrix of hidden node representations at layer ℓ , with $\mathbf{H}^{(0)} = \mathbf{X}$, $\mathbf{W}^{(\ell)} \in \mathbb{R}^{h_\ell \times h_{\ell+1}}$ is a layer-specific learnable weight matrix, $\sigma(\cdot)$ denotes a non-linear activation function, and $\hat{\mathbf{A}}$ is the symmetrically normalized adjacency matrix

$$\hat{\mathbf{A}} = \tilde{\mathbf{D}}^{-\frac{1}{2}} \tilde{\mathbf{A}} \tilde{\mathbf{D}}^{-\frac{1}{2}}. \quad (2)$$

Here, $\tilde{\mathbf{A}} = \mathbf{A} + \mathbf{I}_N$, \mathbf{I}_N is the $N \times N$ identity matrix, $\tilde{\mathbf{D}} = \text{diag}(\sum_j \tilde{\mathbf{A}}_{ij})$. This normalization stabilizes the scale of feature propagation across nodes with varying degrees and can be interpreted as applying a localized spectral filter on the graph.

After stacking L such layers, the final output

$\mathbf{H}^{(L)}$ provides the node representations used for downstream tasks, such as node classification.

3.2 Discrete Ricci Curvature and Ricci Flow

Discrete curvature discretizes notions from differential geometry to quantify the deviation of a graph’s local structure from flatness. Among several discrete analogues of curvature [7, 30–32], the Ollivier-Ricci curvature [5] is widely used, providing a probabilistic interpretation via optimal transport. For an edge $e = (u, v)$, its curvature κ_e is defined as

$$\kappa_e = 1 - \frac{W_1(m_u, m_v)}{\rho_e},$$

where ρ_e is the shortest-path distance between nodes u and v , and $W_1(m_u, m_v)$ is the 1-Wasserstein distance between two probability measures m_u and m_v defined on the neighborhoods of u and v , respectively. Intuitively, positive curvature indicates locally clustered structures, zero curvature suggests flat regions, and negative curvature corresponds to tree-like or bottleneck structures.

On a graph \mathcal{G} with initial edge weights $\{w_e\}_{e \in \mathcal{E}}$, a discrete Ricci flow can be defined to evolve these weights based on edge curvatures. For an edge $e = (u, v)$ with curvature $\kappa_e(t)$ and weight $w_e(t)$ at iteration t , the continuous flow is described by

$$w'_e(t) = -\kappa_e(t)\rho_e(t).$$

In practice, we adopt a discretized version with a step size $\delta > 0$

$$w_e(t+1) = w_e(t) - \delta\kappa_e(t)\rho_e(t). \quad (3)$$

Repeating this process T times, the flow generates a sequence of weighted graphs $\{\mathcal{G}(t)\}_{t=0}^T$ that encodes the multi-scale geometric evolution of the original structure. Note that, from the definitions of κ_e and ρ_e , whenever $\delta \leq 1$, the iter-

actively updated weights $w_e(t+1)$ remain strictly positive, provided that the initial weights $w_e(0)$ are positive.

3.3 Recurrent Neural Networks and Long Short-Term Memory

RNNs offer a natural framework for modeling sequential data, enabling them to process the dynamic graph sequences. However, standard RNNs suffer from the vanishing gradient problem, where gradients diminish exponentially during backpropagation, severely limiting their ability to learn long-range dependencies of the sequence.

LSTMs introduce a gated cell state that enables selective retention and forgetting of information across long sequences. The forget gate determines what information from the previous cell state should be retained or discarded. The input gate regulates the incorporation of new candidate information. The output gate controls which aspects of the updated cell state are propagated to the hidden state. This gating mechanism enables LSTMs to maintain stable gradients over long sequences and selectively preserve long-range dependencies while flexibly integrating new inputs.

This capability makes LSTMs particularly suitable for modeling the geometric evolution sequences produced by discrete Ricci flow. At each iteration of (3), the Wasserstein distance is determined by edge weights and graph random walks. Accordingly, every iteration captures the geometric structure of the graph at a broader scope. Since the LSTM encodes the sequence of curvature generated by Ricci flow, its ability to learn long-range dependencies enables the model to capture multi-scale structural evolution and endows each node with a larger receptive field. The encoded temporal-geometric features are then integrated into subsequent graph convolution layers. This design yields richer and more

expressive node representations than those obtained from standard GCNs operating on static graph snapshots.

4 Methodology

The proposed Geometric Evolution Graph Convolutional Network is designed to unveil the multi-scale structural dynamics of graphs by integrating discrete Ricci flow with sequential deep learning. GEGCN comprises three key components (Figure 1): (i) a Geometric Evolution Generator that produces a graph sequence via discrete Ricci flow; (ii) a Structural Dynamics Encoder based on LSTM; and (iii) a Curvature-aware Graph Convolution module for learning final node representations.

4.1 Geometric Evolution Generator via Discrete Ricci Flow

This module generates a multi-scale geometric evolution of the input graph via discrete Ricci flow. Given an input graph $\mathcal{G} = (\mathcal{V}, \mathcal{E})$, each edge $e \in \mathcal{E}$ is assigned an initial weight $w_e(0)$, which is typically set to 1.

We construct a temporal graph sequence by the discrete Ricci flow. The process begins by computing the initial discrete Ricci curvature $\kappa_e(0)$ for every edge $e \in \mathcal{E}$. We then perform T iterations of the discrete Ricci flow. In each iteration t , after updating the edge weight $w_e(t)$ according to Eq. (3), we recalculate the corresponding Ricci curvature $\kappa_e(t)$ and the shortest-path distance $\rho_e(t)$ based on the updated weighted graph. This iterative procedure produces, for each edge e , two evolution sequences that encode its geometric dynamics. One is the curvature sequence

$$\mathcal{K}_e = [\kappa_e(0), \kappa_e(1), \dots, \kappa_e(T)],$$

and another is the weight sequence

$$\mathcal{W}_e = [w_e(0), w_e(1), \dots, w_e(T)].$$

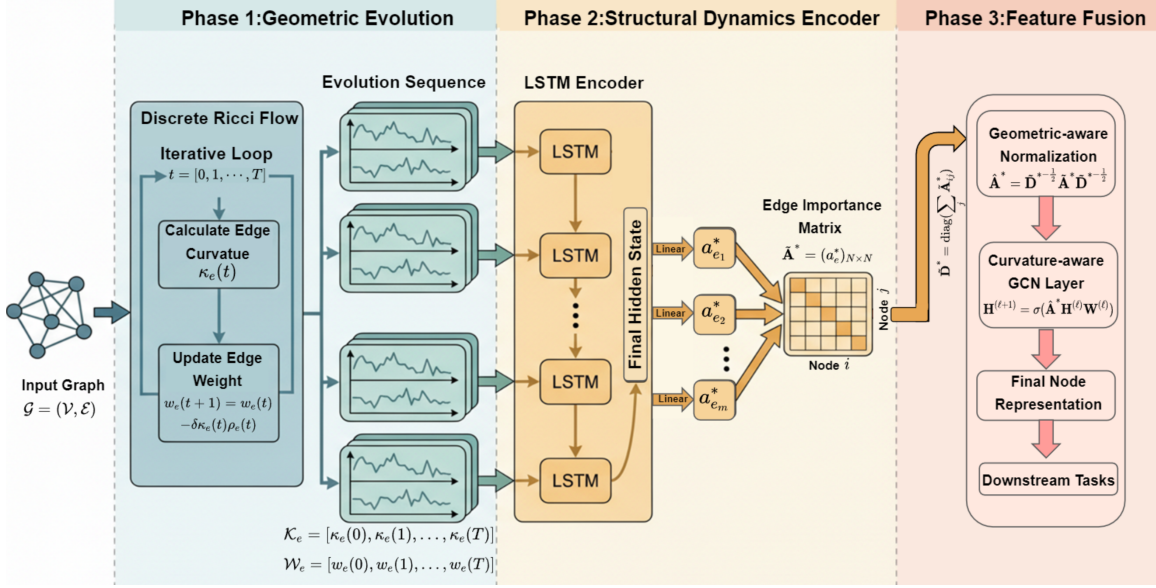


Figure 1: **Overview of the GEGCN framework.** It comprises three phases: (i) Geometric Evolution Generator via Discrete Ricci Flow; (ii) Structural Dynamics Encoder for capturing temporal dynamics and constructing the edge importance matrix via LSTM; and (iii) Feature Fusion for integrating geometric insights into curvature-aware GCN layers.

Conceptually, while the classical Ricci flow on a smooth manifold defines a continuous geometric deformation that preserves fundamental structures, its discrete counterpart in Eq. (3) induces a stepwise evolution of the graph, preserving its underlying adjacency topology.

4.2 Structural Dynamics Encoder Based on LSTM

To learn latent representations of the geometric dynamics, we design an LSTM-based encoder that processes the curvature and weight sequences generated in Sec. 4.1. After the Ricci-flow process on the original edge set \mathcal{E} is completed, we append one self-loop to each node and assign to it a constant curvature sequence 0 and a constant weight sequence 1.

At time step t , the feature vector $\mathbf{x}_e^{(t)} = [\kappa_e(t), w_e(t)]$ of each original edge and appended self-loop is fed into the LSTM cell:

$$\mathbf{h}_e^{(t)}, \mathbf{c}_e^{(t)} = \text{LSTM}(\mathbf{x}_e^{(t)}, \mathbf{h}_e^{(t-1)}, \mathbf{c}_e^{(t-1)}),$$

where $\mathbf{h}_e^{(t)} \in \mathbb{R}^d$ denotes the hidden state, representing the accumulated geometric information up to the current time.

We input the final hidden state $\mathbf{h}_e^{(T)}$ of each edge into an edge-scoring head to output the importance score of the edge. This head consists of a linear transformation followed by a Sigmoid activation:

$$a_e^* = \sigma(\mathbf{W}_s \mathbf{h}_e^{(T)} + b_s),$$

where $a_e^* \in (0, 1)$ is the learned edge importance score. By integrating \mathcal{K}_e and \mathcal{W}_e into the score a_e^* , this module can adaptively emphasize structural information that are persistent or critical across different scales.

4.3 Curvature-aware Graph Convolution

The classical GCN updates the node embedding matrix $\mathbf{H}^{(\ell)}$ to $\mathbf{H}^{(\ell+1)}$ according to Eq. (1). The normalized adjacency matrix $\hat{\mathbf{A}}$ in GCNs relies

on static node degrees via $\tilde{\mathbf{D}}$, treating all edges incident to nodes of the same degree in a uniform manner. This design fails to account for the nuanced geometric hierarchy within the graph.

Discrete Ricci flow provides a much richer, dynamic measure for each edge over time. To integrate this vital geometric information, we propose replacing the static, degree-based normalization matrix $\hat{\mathbf{A}}$ with a geometric-aware normalization matrix. Let $\tilde{\mathbf{A}}^* = (a_e^*)_{N \times N}$ be the edge importance matrix obtained by the LSTM encoder in Sec. 4.2, and $\tilde{\mathbf{D}}^* = \text{diag}(\sum_j \tilde{\mathbf{A}}_{ij}^*)$. The geometric-aware normalization matrix is defined as

$$\hat{\mathbf{A}}^* = \tilde{\mathbf{D}}^{*-1/2} \tilde{\mathbf{A}}^* \tilde{\mathbf{D}}^{*-1/2}.$$

The update at the ℓ -th layer of the curvature-aware graph convolution is defined as

$$\mathbf{H}^{(\ell+1)} = \sigma(\hat{\mathbf{A}}^* \mathbf{H}^{(\ell)} \mathbf{W}^{(\ell)}).$$

We remark that the matrix $\tilde{\mathbf{A}} = \mathbf{A} + \mathbf{I}_N$ in Eq. (2) represents the adjacency matrix after adding a self-loop to every node in the graph. This ensures that each node retains its own features during the message-passing process of GCN. To align with this design, we append one self-loop to each node only after the Ricci-flow process in Sec. 4.1 has been completed on the original edge set. Each appended self-loop is assigned a constant weight of 1 and a constant curvature of 0 at all time steps, and therefore does not affect the curvature or distance computation of the original edges. After normalization by $\tilde{\mathbf{D}}^*$, the self-loop score (the diagonal entry of $\hat{\mathbf{A}}^*$) is jointly determined by the scores of all incident edges of that node and may therefore vary across nodes. This indicates that GEGCN captures the global geometric structure of the graph, leading to heterogeneous levels of self-feature preservation among different nodes.

5 Experiments

5.1 Experimental Setup

Datasets. We perform extensive experiments to validate the performance of GEGCN across a wide range of benchmark datasets, including homophilic/heterophilic graphs, filtered graphs, and large-scale graphs.

For homophilic scenarios, we utilize three citation networks (Cora, Citeseer, and Pubmed [33]), the Coauthor CS network based on the Microsoft Academic Graph from the KDD Cup 2016 challenge, and the Amazon Photos product network [34]. Following the partitioning scheme in [23], we employ **a uniform 20%/10%/70% split for training, validation, and testing.**

To investigate the model’s robustness in heterophilic settings, we extend our evaluation to datasets including Cornell, Texas, and Wisconsin from WebKB [35], as well as Chameleon [36] and Actor [37]. Note that, for these heterophilic benchmarks, we adopt the experimental protocol from [8], **using a 60%/20%/20% data split. And the test set is always fixed rather than randomly sampled,** and the remaining nodes are then randomly divided into training and validation sets. This is to ensure that the test set is not used for any training or hyperparameter tuning prior to final evaluation.

For heterophilic scenarios, to further evaluate the long-range capability and heterophily robustness of our model, and to avoid the train-test data leakage issue reported in [38] on unfiltered datasets, we conduct additional experiments on six heterophilic benchmark datasets proposed in [38], namely filtered Squirrel, filtered Chameleon, Roman-empire, Amazon-ratings, Minesweeper and Questions. For these datasets, we follow **the same data split protocol as [38].**

Finally, to evaluate the long-range capabilities and computational efficiency of GEGCN, we conduct experiments on the large-scale OGBN-arXiv benchmark and report both training and

inference time. On this dataset, we adopted **the standard train/validation/test split provided by OGB [39]**. Specifically, we use papers published until 2017 as the training set, those in 2018 as the validation set, and those published in 2019 and later as the test set.

Comparison Methods. In the evaluation on homophilic datasets, we compare our model against a diverse set of competitive baselines ranging from classical GNNs to spectral-based methods. These include MLP, GCN [2], GAT [3], and GraphSAGE [4]. We also include models designed for deeper or more flexible propagation, such as JKNet [40], APPNP [41], GPRGNN [42], MoNet [43], and UFGConv [44]. Moreover, we consider the geometry-based approaches CurvGN [12] and RC-UFG [23].

For heterophilic benchmarks, the focus shifts to mitigating the oversquashing phenomenon, which attributes to graph bottlenecks characterized by high negative curvature [8]. To this end, we benchmark GEGCN against specialized architectures and graph-rewiring strategies: (i) GCN as a fundamental backbone; (ii) DIGL [45], which employs diffusion to improve graph connectivity; (iii) +FA [46], which introduces a fully adjacent layer to bypass structural bottlenecks; (iv) SDRF¹ [8], a surgical rewiring method based on Discrete Ricci Flow; and (v) GNRF [29], a curvature-informed diffusion method integrating Ricci flow.

For the six heterophilic datasets introduced in [38], we compare against multiple strong baselines employed in [38] and GNRF [29]. Among them, ResNet [47] and GAT [3] are representative neural architectures. H2GCN[48], GPR-GNN[42], GloGNN[49], FS-GNN[50], FAGCN[51], and GBK-GNN[52] are models designed for node classification under heterophily.

¹Note that reproducibility issues regarding the original results have been reported due to incomplete experimental details (Issue). To ensure a fair comparison with our method, we reproduce the experiments of SDRF

On the large-scale OGBN-arXiv dataset, we compare GEGCN with models including MLP, GCN [2], GAT [3], GraphSAGE [4], as well as a random walk-based method Node2vec [53] and strong baselines UniMP [54] and AGDN [55].

For all the above benchmark datasets, the average results of 10 random experiments are reported, and the top **first**, **second**, and **third** are highlighted. Hyperparameters were selected by automated search over the predefined spaces in Appendix C.2, using the mean validation accuracy as the model-selection criterion.

5.2 Main Results

Node Classification in Homophilic Graph.

As demonstrated in TABLE 1, the proposed GEGCN framework consistently achieves superior performance, securing the highest accuracy on four out of five benchmark datasets and ranking second on the remaining one.

Compared to classic message-passing baselines such as GCN, GAT, and GraphSAGE, GEGCN exhibits significant performance gains. For instance, on the Cora and Citeseer networks, our model outperforms the standard GCN by margins of approximately 5.2% and 5.7%, respectively. This substantial improvement can be attributed to the learnable geometric-aware normalization matrix \hat{A}^* . By integrating the Ricci flow sequence via LSTM, our model effectively re-weights edges based on their geometric evolution, allowing for more robust information propagation that goes beyond static topology.

GEGCN also demonstrates a distinct advantage over recent geometric methods like CurvGN, UFGConv, and RC-UFG. Notably, on the Pubmed dataset, GEGCN achieves a top-1 accuracy of 87.4%, surpassing the second-best method, RC-UFG (Hom), by a remarkable margin of 4.5%. While baseline curvature methods typically rely on static curvature or single-snapshot filtering, GEGCN models the entire trajectory of structural evolution through \mathcal{K}_e and \mathcal{W}_e . The LSTM encoder successfully cap-

Table 1: Mean test set classification accuracy (in %) and standard deviation across five homophilic benchmarks.

	Cora	Citeseer	Pubmed	Coauthor CS	Amazon Photos
MLP	55.1±1.4	59.1±1.2	71.4±0.8	88.3±0.7	69.6±3.8
MoNet	81.7±0.4	71.2±0.7	78.6±0.5	90.8±0.6	91.2±1.3
GCN	81.5±0.5	70.9±0.5	79.0±0.3	91.1±0.5	91.2±1.2
GraphSAGE	79.2±7.7	71.6±1.9	77.4±2.2	91.3±2.8	91.4±1.4
GAT	83.0±0.7	72.5±0.7	79.0±0.3	90.5±0.6	85.1±2.3
JKNet	83.7±0.7	72.5±0.4	82.6±0.5	91.1±0.3	86.1±1.1
APPNP	83.5±0.7	75.9±0.6	80.2±0.3	91.5±0.1	87.0±0.9
GPRGNN	83.8±0.9	75.9±0.7	82.3±0.2	91.8±0.1	87.0±0.9
CurvGN	82.6±0.6	71.5±0.8	78.8±0.6	92.9±0.4	92.5±0.5
UFGConv_S	83.0±0.5	71.0±0.6	79.4±0.4	92.1±0.2	92.1±0.5
UFGConv_R	83.6±0.6	72.7±0.6	79.6±0.4	93.0±0.7	92.5±0.2
RC-UFG (Hom)	84.4±0.7	72.5±0.7	82.9±0.2	94.2±0.9	93.5±0.7
RC-UFG (Het)	80.6±0.4	71.7±0.6	79.6±0.4	90.4±1.2	89.5±1.9
GEGCN	86.7±1.2	76.6±1.1	87.4±0.4	93.2±0.4	94.1±0.5

tures the latent dynamics of the Ricci flow process, enabling the model to distinguish between noise and structurally significant connections more effectively than static geometric filters.

Node Classification in Heterophilic Graph.

Table 2 presents the node classification results on five widely adopted heterophilic benchmarks. GEGCN achieves the best results on Chameleon and Actor, with absolute gains of 6.90% and 1.65% over the strongest competing baselines. On the remaining three datasets (Cornell, Texas, Wisconsin), GEGCN ranks second, only inferior to GNRf.

It is notable that the methods relying on global structural modifications, such as diffusion-based preprocessing and curvature-guided rewiring, exhibit dataset-dependent behavior. While these approaches can partially alleviate connectivity sparsity, their performance varies considerably across benchmarks. For instance, DIGL offers limited or inconsistent improvements on Texas and Wisconsin (Table 2), despite enhancing graph connectivity. This suggests that, in heterophilic graphs, increasing connectivity alone is insufficient and may even be detrimental when newly introduced paths

predominantly link nodes with dissimilar labels.

In contrast, GEGCN embeds geometric information into the message-passing process rather than treating it as an external preprocessing step. This design enables curvature to modulate the propagation of information between nodes, rather than altering the graph topology. As a result, GEGCN can selectively amplify task-relevant signals while suppressing misleading aggregation effects that commonly arise in heterophilic settings.

The advantage of this integrated approach is further reflected on Chameleon and Actor. Fully connected or aggressively densified graphs (+FA) fail to deliver comparable gains, despite theoretically eliminating distance-based bottlenecks. This contrast suggests that oversquashing in heterophilic graphs is not only caused by limited information propagation range, but also by indiscriminate aggregation of heterogeneous signals. By evolving the geometry of message passing in a curvature-aware manner, GEGCN provides a more principled mechanism for long-range information flow without sacrificing discriminative locality.

Notably, recent work [38] has identified train-test data leakage issues in the aforementioned

Table 2: Mean test set classification accuracy (%) and standard deviation across heterophilic benchmarks.

	Cornell	Texas	Wisconsin	Chameleon	Actor
GCN	52.69±0.21	61.19±0.49	54.60±0.86	41.33±0.18	23.84±0.43
Undirected	53.20±0.53	63.38±0.87	51.37±1.15	42.02±0.30	21.45±0.47
+FA	58.29±0.49	64.82±0.29	55.48±0.62	42.67±0.17	24.14±0.43
DIGL	58.26±0.50	62.03±0.43	49.53±0.27	42.02±0.13	24.77±0.32
DIGL + Undirected	59.54±0.64	63.54±0.38	52.23±0.54	42.68±0.12	25.45±0.30
SDRF	54.60±0.39	64.46±0.38	55.51±0.27	42.73±0.15	28.42±0.75
SDRF + Undirected	57.54±0.34	67.02±0.40	56.55±0.86	44.46±0.17	28.35±0.06
G NRF	73.05±3.52	83.33±6.08	88.20±3.84	53.82±3.02	35.53±0.68
GEGCN	68.61±0.26	70.27±0.69	67.39±0.93	60.72±0.16	37.18±0.30

heterophilic datasets, which may lead to inflated performance estimates and unfair benchmark comparisons. To further evaluate the heterophily robustness and to avoid the leakage issue, we conduct additional experiments on the six heterophilic benchmarks without the train-test data leakage issue [38]. As shown in Table 3, GEGCN achieves SOTA on three out of six benchmarks, ranks second on Questions and Squirrel-f, and takes third place on Chameleon-f. In particular, on the Roman-empire dataset, GEGCN outperforms the strong baseline GAT by a significant margin. It is worth highlighting that G NRF, which delivers competitive performance on the unfiltered datasets, exhibits notably degraded performance on these rigorously filtered benchmarks. These comprehensive results consistently confirm that GEGCN can effectively capture the intrinsic structural properties of heterophilic graphs, and maintains robust competitive performance across both unfiltered and rigorously filtered heterophilic benchmarks.

To evaluate the long-range capabilities and computational efficiency of GEGCN, we also conduct experiments on the OGBN-arXiv benchmark, which is a typical large-scale sparse graph with complex long-range topological correlations among nodes. On OGBN-arXiv, we compare GEGCN with representative baselines covering multiple mainstream categories. Experimental results (Table 4) demonstrate that GEGCN

achieves competitive SOTA performance on this large-scale benchmark.

The promising performance of GEGCN indicates that the geometric evolution combined with LSTM effectively captures long-range dependencies across distant node hops. The superior performance on OGBN-arXiv also validates the superiority and generalization ability of GEGCN on real-world large-scale graph scenarios. We further report the training and inference time of all compared models in Section 5.3, demonstrating that GEGCN maintains acceptable computational overhead while achieving outstanding prediction accuracy.

Overall, all these results suggest that by embedding geometric evolution within the convolution process, GEGCN consistently yields competitive results across various experimental settings, including homophilic and heterophilic graphs, filtered benchmark variants, and the large-scale OGBN-arXiv dataset. This cross-consistent performance proves that GEGCN possesses strong generalization and adaptive ability to handle diverse graph topological characteristics, rather than only fitting well on specific dataset types.

Ablation Studies. To investigate the specific contribution of each component within the GEGCN framework to the overall performance, we conduct ablation experiments across the Ac-

Table 3: Mean test set classification accuracy (%) and standard deviation across filtered benchmarks.

	Roman-empire	Amazon-ratings	Minesweeper	Questions	Squirrel-f	Chameleon-f
ResNet	65.88±0.38	45.90±0.52	50.89±1.39	70.34±0.76	36.55±1.82	36.73±4.71
GAT	80.87±0.30	49.09±0.63	92.01±0.68	77.43±1.20	35.62±2.06	39.21±3.08
H2GCN	60.11±0.52	36.47±0.23	89.71±0.31	63.59±1.46	35.10±1.15	26.75±3.64
GPR-GNN	64.85±0.27	44.88±0.34	86.24±0.61	55.48±0.91	35.11±1.24	25.90±3.58
GloGNN	59.63±0.69	36.89±0.14	51.08±1.23	65.74±1.19	35.51±1.65	39.61±2.60
FSGNN	79.92±0.56	52.74±0.83	90.08±0.70	78.86±0.92	35.92±1.32	40.61±2.97
FAGCN	65.22±0.56	44.12±0.30	88.17±0.73	77.24±1.26	38.95±1.99	39.93±3.30
GBK-GNN	74.57±0.47	45.98±0.71	90.85±0.58	74.47±0.86	41.08±2.27	41.90±2.72
GNRF	79.72±0.77	40.04±0.95	84.81±1.25	70.38±3.75	31.35±1.79	34.77±2.33
GEGCN	86.74±1.02	52.77±0.73	92.25±0.93	77.73±0.41	40.03±1.71	40.53±1.81

Table 4: Mean test set classification accuracy (%) and standard deviation on OGBN-arXiv.

	Test Accuracy
MLP	57.65±0.12
Node2vec	71.29±0.13
GraphSAGE	72.77±0.16
GCN	73.00±0.17
GAT	73.30±0.16
UniMP	74.50±0.05
AGDN	75.22±0.07
GEGCN	75.76±0.64

tor, Cornell, and Wisconsin datasets. We design three groups of ablated variants to verify the effectiveness of different modules. First, we adopt the standard GCN as the baseline, which removes both the Ricci flow curvature evolution module and the LSTM encoder. Second, we preserve the Ricci flow module and replace the LSTM with several pooling strategies for modeling curvature sequences, including taking the first element, the last element, the average value, and the maximum value of the curvature sequence. Third, we keep the architectural pipeline of GEGCN and merely substitute the LSTM encoder with an MLP. It should be remarked that, our MLP variant only replaces the LSTM encoder while still inherits the overall framework of GEGCN. It is fundamentally different from the GNRF architecture, which builds upon the diffusion equation coupled with

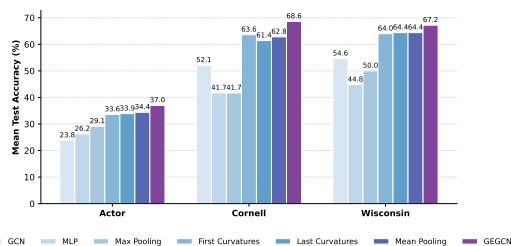


Figure 2: **Ablation Study.** The bar chart compares the mean test accuracy (%) of the baseline GCN, five ablation variants that replace the LSTM module for modeling Ricci curvature evolution with First, Last, Mean Pooling, Max Pooling, or MLP-based aggregation, and the full GEGCN model. The consistent performance gains of GEGCN across all datasets demonstrate the effectiveness of LSTM-based modeling of the Ricci curvature evolution sequence.

an MLP-based EdgeNet.

As presented in Figures 2, GEGCN consistently achieves superior results compared to all ablated variants, underscoring the necessity of integrating geometric evolution into GCN.

The baseline GCN achieves the lowest accuracy on the Actor dataset, reaching only 23.8%, while the curvature-aware variants generally provide stronger performance when the curvature evolution is summarized effectively. Simple replacements of the LSTM module, including First, Last, Mean Pooling, Max Pooling, and MLP-based aggregation, offer different ways to use Ricci curvature information, but their per-

formance varies across datasets. In contrast, the full GEGCN model achieves the best results on all three datasets, with 37.0% on Actor, 68.6% on Cornell, and 67.2% on Wisconsin. This consistent advantage shows that explicitly modeling the Ricci curvature evolution sequence with the LSTM encoder is more effective than using static snapshots or simple aggregation strategies, leading to better representations for graph learning.

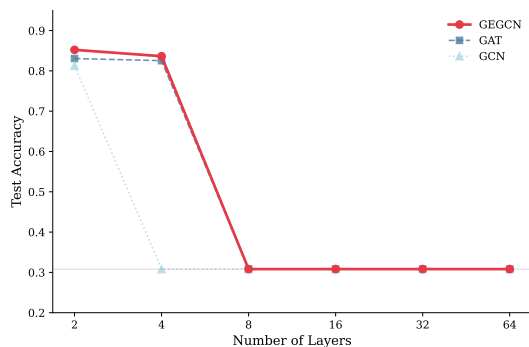


Figure 3: **Oversmoothing analysis on Cora.** We report the mean test accuracy across various numbers of layers $L \in \{2, 4, 8, 16, 32, 64\}$. All models eventually collapse to the chance level (30.82%), but GEGCN maintains significantly higher accuracy at $L = 4$ compared to the vanilla GCN.

Analysis of Oversmoothing. A well-known drawback of GCNs is that capturing long-range dependencies by adding layers comes at the cost of oversmoothing. To investigate the susceptibility of the proposed model to the oversmoothing phenomenon, we report the test accuracy on the Cora dataset across varying depths $L \in \{2, 4, \dots, 64\}$ in Figure 3. While all models eventually converge to the chance level (30.82%), GEGCN exhibits superior resilience compared to GCN. Notably, GCN experiences a catastrophic performance collapse as early as $L = 4$, whereas GEGCN maintains its discriminative power with a high accuracy of 83.64%. Furthermore, GEGCN consistently outperforms GAT at manageable depths ($L \leq 4$), suggesting that

its structural priors effectively delay the convergence of node representations into an indistinguishable subspace. This extended effective depth range enables GEGCN to integrate long-range information while maintaining feature diversity, which is a common limitation in standard GNNs where features tend to homogenize rapidly.

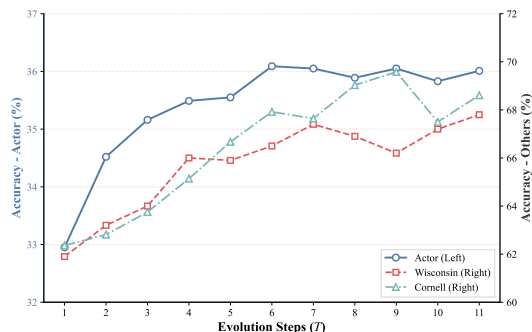


Figure 4: **Sensitivity analysis of evolution steps (T).** The node classification accuracy across three heterophilic datasets (Actor, Wisconsin, and Cornell) generally improves as the Ricci flow evolution length T increases, demonstrating the advantage of capturing long-term geometric refinement. The performance tends to stabilize after $T = 6$, indicating a saturation of geometric information extraction.

Impact of Ricci Flow Duration As illustrated in Figure 4, we analyze the impact of the discrete Ricci flow step count T on the performance of our model. We observe a consistent accuracy gain as T increases from 1 to 6 across three datasets. This trend suggests that GEGCN successfully leverages the temporal curvature sequences to identify complex structural patterns that are otherwise invisible in a static graph snapshot. Specifically, the Actor dataset exhibits the most significant improvement, likely due to its highly sparse nature, which requires more evolution steps to reveal underlying homophily clusters.

5.3 Computational Complexity

The computational complexity of the geometric evolution process is mainly dominated by the calculation of the 1-Wasserstein distance for each edge. Exact solvers for this linear programming problem generally yield a complexity of $O(|E|D^3)$, where D denotes the average node degree. Such a computational cost can be prohibitively expensive on large-scale graphs, yet this issue is effectively alleviated by adopting the Sinkhorn algorithm [56]. With entropic regularization incorporated, the complexity is reduced to nearly $O(|E|D^2)$. In addition, shortest-path re-computation is required after each edge weight update, which costs $O(|V|(|E| + |V| \log |V|))$ per iteration via the Dijkstra algorithm. For dense or moderately sparse graphs, the $O(|E|D^2)$ term dominates the overall computational overhead. Furthermore, the discrete Ricci flow is implemented as a one-time pre-processing step (see the execution time in Appendix C.4), which is decoupled from the neural network training. Consequently, the online training phase only accounts for the LSTM encoder and GCN layers, both of which are linear with respect to the number of edges, ensuring the overall GEGCN framework remains efficient and feasible for practical applications.

Table 5: The average training and inference time of GEGCN across seven datasets.

	Train (s)	Inf. (s)
Chameleon-f	34.62	0.078
Minesweeper	137.90	0.574
Squirrel-f	153.96	0.597
Roman-empire	158.84	0.353
Amazon-ratings	244.22	1.357
Questions	457.05	1.759
OGBN-arXiv	732.90	14.557

To further assess the computational efficiency of GEGCN, we report its average training and inference time across the seven datasets in Table 5. Even on the large-scale OGBN-arXiv, the training and inference time is efficiently bounded.

The acceptable computational efficiency and stable performance on various graphs further illustrate that GEGCN has good practical deployment potential for real large-scale graphs.

6 Conclusion

The core idea of this paper is to model the evolutionary sequences generated by Ricci flow as a temporal process and integrate it seamlessly into a graph deep learning framework. Our framework consists of three stages: (i) We first apply discrete Ricci flow to the input graph to generate multi-scale geometric sequences. (ii) An LSTM encoder is then employed to process this sequence, learning to encode the trajectory of geometric changes into a compact representation. (iii) Finally, these geometric-aware representations are infused as enhanced features into a standard GCN, which performs the downstream prediction tasks. This design allows GEGCN to simultaneously leverage local neighborhood information (via GCN) and global, multi-scale geometric dynamics (via Ricci flow and LSTM). As a result, GEGCN demonstrates superior node representation learning capability. Extensive experiments on a broad range of benchmark datasets demonstrate the strong effectiveness and competitiveness of the proposed method. More broadly, GEGCN offers a modular perspective on geometry-aware graph learning: rather than treating curvature as a static descriptor or relying solely on topology rewiring, it models geometric evolution as a learnable sequential signal and integrates the resulting structural dynamics directly into message passing. We hope this perspective will provide a principled bridge between discrete geometric analysis and neural graph representation learning, and inspire future graph architectures that make fuller use of geometric dynamics.

Impact Statement

This paper presents the Geometric Evolution Graph Convolutional Network (GEGCN), a novel framework that enhances graph representation learning by modeling geometric evolution on graphs. There are many potential societal consequences of our work, none of which we feel must be specifically highlighted here.

References

1. Zhou J, Cui G, Hu S, et al. Graph Neural Networks: A Review of Methods and Applications. *AI Open* 2020;1:57–81.
2. Kipf TN and Welling M. Semi-supervised classification with graph convolutional networks. In: *International Conference on Learning Representations*. 2017.
3. Veličković P, Cucurull G, Casanova A, Romero A, Lio P, and Bengio Y. Graph attention networks. In: *International Conference on Learning Representations*. 2018.
4. Hamilton WL, Ying R, and Leskovec J. Inductive representation learning on large graphs. In: *Proceedings of the 31st International Conference on Neural Information Processing Systems*. Long Beach, California, USA: Curran Associates Inc., 2017:1025–35.
5. Ollivier Y. Ricci curvature of Markov chains on metric spaces. *Journal of Functional Analysis* 2009;256:810–64.
6. Forman R. Bochner’s method for cell complexes and combinatorial Ricci curvature. *Discrete & Computational Geometry* 2003;29:323–74.
7. Lin Y, Lu L, and Yau ST. Ricci curvature of graphs. *Tohoku Mathematical Journal* 2011;63:605–27.
8. Topping J, Di Giovanni F, Chamberlain BP, Dong X, and Bronstein MM. Understanding over-squashing and bottlenecks on graphs. In: *International Conference on Learning Representations*. 2022.
9. Ni CC, Lin YY, Luo F, and Gao J. Community Detection on Networks with Ricci Flow. *Scientific Reports* 2019;9:9984.
10. Lai X, Bai S, and Lin Y. Normalized Discrete Ricci Flow used in Community Detection. *Physica A: Statistical Mechanics and its Applications* 2022;597:127251.
11. Sandhu RS, Georgiou TT, Reznik E, et al. Graph Curvature for Network Fragility: An Application to Financial Markets. *Science Advances* 2016;2:e1501495.
12. Ye Z, Liu KS, Ma T, Gao J, and Chen C. Curvature Graph Network. In: *International Conference on Learning Representations*. 2020.
13. Liu Y, Zhou C, Pan S, et al. CurvDrop: A Ricci Curvature Based Approach to Prevent Graph Neural Networks from Over-Smoothing and Over-Squashing. In: *Proceedings of the ACM Web Conference 2023*. WWW ’23. Austin, TX, USA, 2023:221–30.
14. Bauer F, Jost J, and Liu S. Ollivier-Ricci curvature and the spectrum of the normalized graph Laplace operator. *Mathematical Research Letters* 2012;19:1185–205.
15. Bai S, Lin Y, Lu L, Wang Z, and Yau ST. Ollivier Ricci-flow on weighted graphs. *American Journal of Mathematics* 2024;146:1723–47.
16. Ma J and Yang Y. A modified Ricci flow on arbitrary weighted graph. *The Journal of Geometric Analysis* 2025;35:332.
17. Ni CC, Lin YY, Gao J, and Gu X. Network Alignment by Discrete Ollivier-Ricci Flow. In: *Graph Drawing and Network Vi-*

- sualization*. Cham: Springer International Publishing, 2018:447–62.
18. Tian Y, Ma J, Yang Y, and Zhao L. Community detection of undirected hypergraphs by Ricci flow. *Physical Review E* 4 2025;112:044311.
 19. Hochreiter S and Schmidhuber J. Long Short-Term Memory. *Neural Computation* 1997;9:1735–80.
 20. Li H, Cao J, Zhu J, Liu Y, Zhu Q, and Wu G. Curvature Graph Neural Network. *Information Sciences* 2022;592:50–66.
 21. Yang M, Zhou M, Pan L, and King I. κ HGCN: Tree-likeness Modeling via Continuous and Discrete Curvature Learning. In: *Proceedings of the 29th ACM SIGKDD Conference on Knowledge Discovery and Data Mining*. KDD '23. Long Beach, CA, USA: Association for Computing Machinery, 2023:2965–77.
 22. Sun L, Ye J, Peng H, and Yu PS. A Self-supervised Riemannian GNN with Time Varying Curvature for Temporal Graph Learning. In: *Proceedings of the 31st ACM International Conference on Information & Knowledge Management*. CIKM '22. Atlanta, GA, USA: Association for Computing Machinery, 2022:1827–36.
 23. Shi D, Guo Y, Shao Z, and Gao J. How curvature enhance the adaptation power of framelet GCNs. arXiv preprint arXiv:2307.09768 2023.
 24. Nguyen K, Hieu NM, Nguyen VD, Ho N, Osher S, and Nguyen TM. Revisiting Over-smoothing and Over-squashing Using Ollivier-Ricci Curvature. In: *Proceedings of the 40th International Conference on Machine Learning*. Vol. 202. Proceedings of Machine Learning Research. PMLR, 2023:25956–79.
 25. Giraldo JH, Skianis K, Bouwmans T, and Malliaros FD. On the Trade-off between Over-smoothing and Over-squashing in Deep Graph Neural Networks. In: *Proceedings of the 32nd ACM International Conference on Information and Knowledge Management*. CIKM '23. Birmingham, United Kingdom: Association for Computing Machinery, 2023:566–76.
 26. Fu X, Wang J, Gao Y, et al. Discrete Curvature Graph Information Bottleneck. *Proceedings of the AAAI Conference on Artificial Intelligence* 2025;39:16666–73.
 27. Chamberlain B, Rowbottom J, Gorinova MI, Bronstein M, Webb S, and Rossi E. GRAND: Graph Neural Diffusion. In: *International Conference on Machine Learning (ICML) / PMLR*. Vol. 139. 2021:1407–18.
 28. Chamberlain BP, Rowbottom J, Eynard D, Di Giovanni F, Dong X, and Bronstein MM. Beltrami flow and neural diffusion on graphs. In: *Proceedings of the 35th International Conference on Neural Information Processing Systems*. Vol. 34. Red Hook, NY, USA: Curran Associates Inc., 2021:1594–609.
 29. Chen J, Deng B, WANG Z, Chen C, and Zheng Z. Graph Neural Ricci Flow: Evolving Feature from a Curvature Perspective. In: *International Conference on Learning Representations*. 2025.
 30. Menger K. Untersuchungen über allgemeine Metrik. *Mathematische Annalen* 1930;103:466–501.
 31. Haantjes J. Discrete geometry: curvature in abstract metric spaces. *Proc. Kon. Ned. Akad. v. Wetenseh.* 1947;50:302–14.
 32. Bakry D and Émery M. Hypercontractivité de semigroupes de diffusion. *C. R. Acad. Sci. Paris Sér. I Math.* 1984;299:775–8.

33. Sen P, Namata G, Bilgic M, Getoor L, Gallagher B, and Eliassi-Rad T. Collective Classification in Network Data. *AI Magazine* 2008;29:93–106.
34. McAuley J, Targett C, Shi Q, and Hengel A van den. Image-Based Recommendations on Styles and Substitutes. In: *Proceedings of the 38th International ACM SIGIR Conference on Research and Development in Information Retrieval*. SIGIR '15. Santiago, Chile, 2015:43–52.
35. Craven M, DiPasquo D, Freitag D, et al. Learning to extract symbolic knowledge from the World Wide Web. In: *Proceedings of the Fifteenth National/Tenth Conference on Artificial Intelligence/Innovative Applications of Artificial Intelligence*. AAAI '98/IAAI '98. Madison, Wisconsin, USA, 1998:509–16.
36. Rozemberczki B, Allen C, and Sarkar R. Multi-scale attributed node embedding. *Journal of Complex Networks* 2021;9:cnab014.
37. Tang J, Sun J, Wang C, and Yang Z. Social influence analysis in large-scale networks. In: *Proceedings of the 15th ACM SIGKDD International Conference on Knowledge Discovery and Data Mining*. KDD '09. Paris, France: Association for Computing Machinery, 2009:807–16.
38. Platonov O, Kuznedelev D, Diskin M, Babenko A, and Prokhorenkova L. A critical look at the evaluation of GNNs under heterophily: Are we really making progress? In: *The Eleventh International Conference on Learning Representations*. 2023.
39. Hu W, Fey M, Zitnik M, et al. Open Graph Benchmark: Datasets for Machine Learning on Graphs. In: *Advances in Neural Information Processing Systems*. Vol. 33. Curran Associates, Inc., 2020:22118–33.
40. Xu K, Li C, Tian Y, Sonobe T, Kawarabayashi Ki, and Jegelka S. Representation learning on graphs with jumping knowledge networks. In: *International Conference on Machine Learning (ICML) / PMLR*. 2018:5453–62.
41. Gasteiger J, Bojchevski A, and Günnemann S. Predict then propagate: Graph neural networks meet personalized pagerank. In: *International Conference on Learning Representations*. 2019.
42. Chien E, Peng J, Li P, and Milenkovic O. Adaptive universal generalized pagerank graph neural network. In: *International Conference on Learning Representations*. 2021.
43. Monti F, Boscaini D, Masci J, Rodola E, Svoboda J, and Bronstein MM. Geometric deep learning on graphs and manifolds using mixture model cnns. In: *Proceedings of the IEEE conference on computer vision and pattern recognition*. 2017:5115–24.
44. Zheng X, Zhou B, Gao J, et al. How Framelets Enhance Graph Neural Networks. In: *International Conference on Machine Learning (ICML) / PMLR*. 2021:12761–71.
45. Gasteiger J, Weißenberger S, and Günnemann S. Diffusion improves graph learning. In: *Proceedings of the 33rd International Conference on Neural Information Processing Systems*. Red Hook, NY, USA: Curran Associates Inc., 2019:13366–78.
46. Alon U and Yahav E. On the bottleneck of graph neural networks and its practical implications. In: *International Conference on Learning Representations*. 2021.
47. He K, Zhang X, Ren S, and Sun J. Deep Residual Learning for Image Recognition. In: *2016 IEEE Conference on Computer*

- Vision and Pattern Recognition (CVPR)*. 2016:770–8.
48. Zhu J, Yan Y, Zhao L, Heimann M, Akoglu L, and Koutra D. Beyond homophily in graph neural networks: current limitations and effective designs. In: *Proceedings of the 34th International Conference on Neural Information Processing Systems*. NIPS '20. Vancouver, BC, Canada: Curran Associates Inc., 2020.
 49. Li X, Zhu R, Cheng Y, et al. Finding Global Homophily in Graph Neural Networks When Meeting Heterophily. In: *Proceedings of the 39th International Conference on Machine Learning*. Vol. 162. Proceedings of Machine Learning Research. PMLR, 2022:13242–56.
 50. Maurya SK, Liu X, and Murata T. Simplifying approach to node classification in Graph Neural Networks. *Journal of Computational Science* 2022;62:101695.
 51. Bo D, Wang X, Shi C, and Shen H. Beyond Low-frequency Information in Graph Convolutional Networks. In: *AAAI*. AAAI Press, 2021.
 52. Du L, Shi X, Fu Q, et al. GBK-GNN: Gated Bi-Kernel Graph Neural Networks for Modeling Both Homophily and Heterophily. In: *Proceedings of the ACM Web Conference 2022*. WWW '22. Virtual Event, Lyon, France: Association for Computing Machinery, 2022:1550–8.
 53. Grover A and Leskovec J. Node2Vec: Scalable feature learning for networks. In: *Proceedings of the 22nd ACM SIGKDD international conference on Knowledge discovery and data mining*. 2016:855–64.
 54. Shi Y, Huang Z, Feng S, Zhong H, Wang W, and Sun Y. Masked Label Prediction: Unified Message Passing Model for Semi-Supervised Classification. In: *Proceedings of the Thirtieth International Joint Conference on Artificial Intelligence, IJCAI-21*. Ed. by Zhou ZH. International Joint Conferences on Artificial Intelligence Organization, 2021:1548–54.
 55. Sun C, Zhang M, Hu J, Gu H, Chen J, and Yang M. Adaptive graph diffusion networks: compact and expressive GNNs with large receptive fields. *Artificial Intelligence Review* 2025;58:Article number 107.
 56. Cuturi M. Sinkhorn distances: lightspeed computation of optimal transport. In: *Proceedings of the 27th International Conference on Neural Information Processing Systems*. Vol. 2. Lake Tahoe, Nevada: Curran Associates Inc., 2013:2292–300.
 57. Pei H, Wei B, Chang KWC, Lei Y, and Yang B. Geom-GCN: Geometric Graph Convolutional Networks. In: *International Conference on Learning Representations*. 2020.

A Discrete Ricci Curvature and Ricci Flow

A.1 Summary of Notation

Notation	Description
$\mathcal{G} = (\mathcal{V}, \mathcal{E})$	Graph with node set \mathcal{V} and edge set \mathcal{E}
w_e	Weight of edge $e \in \mathcal{E}$
κ_e	Ricci curvature of edge $e \in \mathcal{E}$
ρ_e	Distance between nodes u and v of an edge $e = (u, v)$
$\mathcal{N}(v)$	Neighborhood of node v
m_v	Probability measure on neighbors of v
δ	Step size for discrete Ricci flow

A.2 Ollivier-Ricci Curvature on Graphs

Various notions of Ricci curvature have been proposed for graphs, with the aim of capturing their geometric and topological properties, including Forman-Ricci curvature [6], Menger-Ricci curvature [30], Haantjes-Ricci curvature [31], and Bakry-Émery Ricci curvature [32]. Among the various definitions proposed in the literature, Ollivier-Ricci curvature [5], with its foundation in optimal transport theory and clear geometric meaning, has gained significant prominence. It quantifies curvature by measuring the transportation cost of probability measures centered at adjacent nodes. In this work, we focus on Ollivier-Ricci curvature as our primary notion of discrete Ricci curvature.

Let $\mathcal{G} = (\mathcal{V}, \mathcal{E})$ be a graph with node set $\mathcal{V} = \{v_1, \dots, v_N\}$ and edge set $\mathcal{E} \subseteq \mathcal{V} \times \mathcal{V}$. Each edge $e \in \mathcal{E}$ is assigned an edge weight w_e . The distance between two nodes u and v is

$$\rho_{uv} = \inf_{\gamma} \sum_{e \in \gamma} w_e,$$

where γ ranges over all paths connecting u and v . For a random walk with parameter $\alpha \in [0, 1]$, the probability measure centered at $u \in \mathcal{V}$ is

$$m_u^\alpha(v) = \begin{cases} \alpha, & v = u, \\ (1 - \alpha) \frac{w_{uv}}{\sum_{z \sim u} w_{zu}}, & v \sim u, \\ 0, & \text{otherwise.} \end{cases}$$

For two probability measures m_u^α, m_v^α on \mathcal{V} , a coupling $A : \mathcal{V} \times \mathcal{V} \rightarrow [0, 1]$ satisfies

$$\sum_{y \in \mathcal{V}} A(x, y) = m_u^\alpha(x), \quad \sum_{x \in \mathcal{V}} A(x, y) = m_v^\alpha(y).$$

The Wasserstein distance between m_u^α and m_v^α is

$$W(m_u^\alpha, m_v^\alpha) = \inf_A \sum_{x, y \in \mathcal{V}} A(x, y) \rho_{xy}.$$

Ollivier-Ricci curvature of edge $e = (u, v)$ is defined as

$$\kappa_e^\alpha = 1 - \frac{W(m_u^\alpha, m_v^\alpha)}{\rho_e}.$$

From a geometric perspective, positive Ollivier-Ricci curvature indicates a significant overlap between the neighborhoods of u and v , implying a local tendency of information or mass to concentrate, analogous to the convergence of geodesics on positively curved manifolds. In contrast, negative curvature corresponds to a separation of neighborhoods and a rapid spreading of information, mirroring the exponential divergence of geodesics in negatively curved spaces. Zero curvature represents a balanced configuration in which neither contraction nor expansion dominates, akin to the flat geometry of Euclidean space. Figure 5 illustrates these interpretations by comparing continuous manifolds and discrete graphs with negative, zero, and positive Ollivier-Ricci curvature. The top row presents representative surfaces from continuous geometry, while the bottom row shows graph structures exhibiting the corresponding curvature behaviors, thereby providing an intuitive correspondence between the continuous and discrete settings.

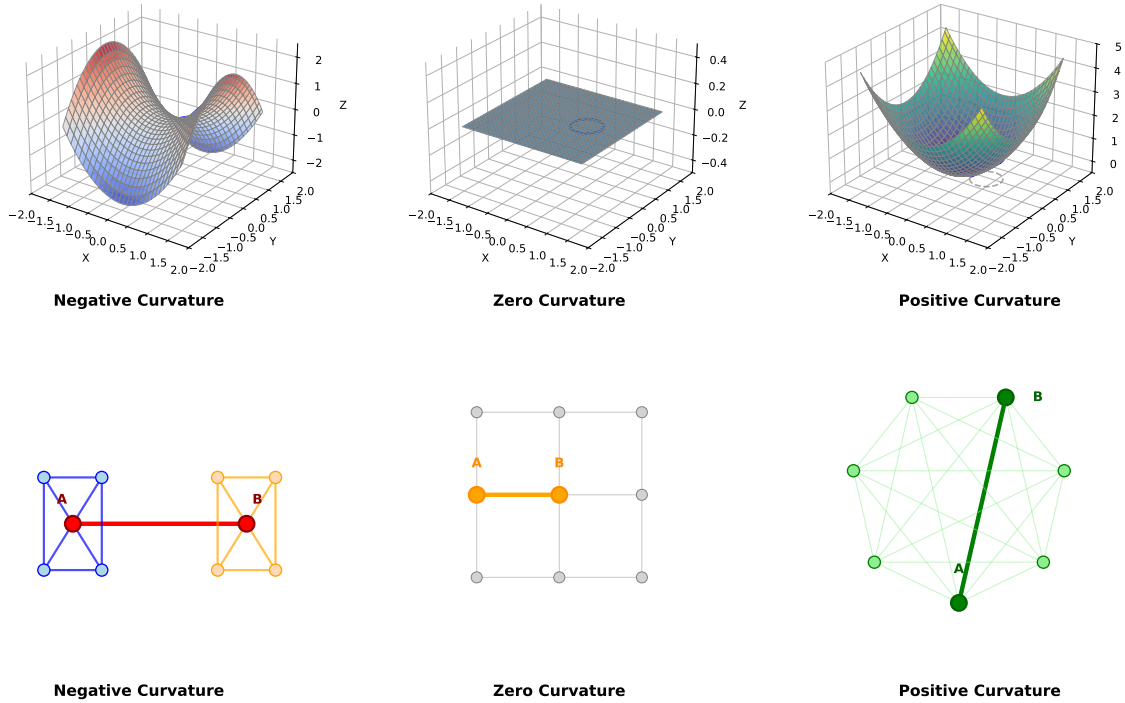


Figure 5: **Comparison of Ollivier-Ricci curvature in continuous manifolds and discrete graphs.** (Top row) Continuous manifolds: (Left) Hyperbolic paraboloid with negative curvature ($\kappa < 0$); (Middle) Plane with zero curvature ($\kappa = 0$); (Right) Elliptic paraboloid with positive curvature ($\kappa > 0$). (Bottom row) Discrete graphs: (Left) Two dense clusters connected by a single edge with negative curvature; (Middle) Regular 3×3 grid with zero curvature; (Right) Complete graph K_7 with positive curvature. All edge weights are set to 1.

A.3 Discrete Ricci Flow

In the smooth setting, Ricci flow provides a fundamental geometric mechanism to evolve the Riemannian metric, which plays a central role in geometric analysis. Ollivier [5] first observed that a discrete analogue of the Ricci flow on manifolds can be formulated on weighted graphs,

$$w'_e(t) = -\kappa_e(t) w_e(t), \quad \forall e \in \mathcal{E},$$

where $\kappa_e(t)$ denotes the Ollivier-Ricci curvature of edge e at time t . Subsequently, Bai et al. [15] replaced the curvature term $\kappa_e(t)$ in the flow equation by the Lin-Lu-Yau Ricci curvature [7], which is a limiting version of Ollivier-Ricci curvature. Bai et al. [15] established the local existence and uniqueness of solutions to this discrete Ricci flow. In particular, they proved the long time existence (up to surgeries) of solutions under an exit condition. More recently, Ma and Yang [16] proposed a modified formulation in which the edge weight $w_e(t)$ on the right-hand side is replaced by the distance $\rho_e(t)$, namely,

$$w'_e(t) = -\kappa_e(t) \rho_e(t), \quad e \in \mathcal{E}.$$

This formulation preserves the essential intuition of the Ricci flow. Along the flow, edges with positive curvature tend to shrink, while those with negative curvature tend to expand. At the same time, the initial value problem has a unique global solution without the exit condition. Therefore, in this work, we adopt this latter formulation as our discrete Ricci flow model for networks.

B Mathematical Expressions of GEGCN

B.1 Geometric Evolution Generator via Discrete Ricci Flow

Let $\mathcal{G} = (\mathcal{V}, \mathcal{E})$ be an undirected graph with initial edge weight $w_e(0)$ for each edge $e \in \mathcal{E}$. The discrete Ricci flow is computed only on the original edge set \mathcal{E} . At time step t , the Ollivier-Ricci curvature $\kappa_e(t)$ and $\rho_e(t)$ of an edge $e = (u, v)$ is computed according to the current weights. The discrete Ricci flow evolves edge weights according to

$$w_e(t+1) = w_e(t) - \delta \kappa_e(t) \rho_{uv}(t), \quad t = 0, \dots, T-1,$$

where $\delta > 0$ is the step size. This process produces a curvature evolution sequence for each edge e ,

$$\mathcal{K}_e = \{\kappa_e(0), \kappa_e(1), \dots, \kappa_e(T)\},$$

and a corresponding weight evolution sequence

$$\mathcal{W}_e = \{w_e(0), w_e(1), \dots, w_e(T)\}.$$

After the Ricci-flow process is completed, we append one self-loop to each node to match the standard GCN design. Each appended self-loop is assigned the constant curvature sequence $\{0, \dots, 0\}$ and the constant weight sequence $\{1, \dots, 1\}$. These self-loops are used only when constructing $\tilde{\mathbf{A}}^*$ and do not affect the curvature, distance, or weight computation of the original edges.

B.2 Structural Dynamics Encoding via LSTM

For each edge $e \in \mathcal{E}$ (including the added self-loop on each node) and each time step t , the curvature and weight are concatenated to form the LSTM input $\mathbf{x}_e^{(t)} = [\kappa_e(t), w_e(t)] \in \mathbb{R}^2$.

The LSTM encoder updates the hidden state $a_e(t)$ and cell state $\mathbf{c}_e(t)$ as

$$\begin{aligned} \mathbf{f}_e^{(t)} &= \sigma(\mathbf{W}_f \mathbf{x}_e^{(t)} + \mathbf{U}_f \mathbf{h}_e^{(t-1)} + \mathbf{b}_f), \\ \mathbf{i}_e^{(t)} &= \sigma(\mathbf{W}_i \mathbf{x}_e^{(t)} + \mathbf{U}_i \mathbf{h}_e^{(t-1)} + \mathbf{b}_i), \\ \mathbf{o}_e^{(t)} &= \sigma(\mathbf{W}_o \mathbf{x}_e^{(t)} + \mathbf{U}_o \mathbf{h}_e^{(t-1)} + \mathbf{b}_o), \\ \tilde{\mathbf{c}}_e^{(t)} &= \tanh(\mathbf{W}_c \mathbf{x}_e^{(t)} + \mathbf{U}_c \mathbf{h}_e^{(t-1)} + \mathbf{b}_c), \\ \mathbf{c}_e^{(t)} &= \mathbf{f}_e^{(t)} \odot \mathbf{c}_e^{(t-1)} + \mathbf{i}_e^{(t)} \odot \tilde{\mathbf{c}}_e^{(t)}, \\ \mathbf{h}_e^{(t)} &= \mathbf{o}_e^{(t)} \odot \tanh(\mathbf{c}_e^{(t)}), \end{aligned}$$

where $\sigma(\cdot)$ denotes the sigmoid function and \odot is the element-wise product. We input the final hidden state $\mathbf{h}_e^{(T)}$ of each edge into an edge-scoring head as:

$$a_e^* = \sigma(\mathbf{W}_s \mathbf{h}_e^{(T)} + b_s),$$

where $a_e^* \in (0, 1)$ is taken as the edge importance score of edge e .

B.3 Geometric-aware Adjacency Normalization

Let $\tilde{\mathbf{A}}^* \in \mathbb{R}^{N \times N}$ denote the edge importance matrix,

$$\tilde{\mathbf{A}}_{ij}^* = \begin{cases} a_e^*, & e \in \mathcal{E}, \text{ or } e \text{ is a self-loop,} \\ 0, & \text{otherwise.} \end{cases}$$

The corresponding degree matrix is

$$\tilde{\mathbf{D}}^* = \text{diag}\left(\sum_j \tilde{\mathbf{A}}_{ij}^*\right).$$

The geometric-aware normalized adjacency matrix is then defined as

$$\hat{\mathbf{A}}^* = \tilde{\mathbf{D}}^{*-1/2} \tilde{\mathbf{A}}^* \tilde{\mathbf{D}}^{*-1/2}.$$

B.4 GEGCN Forward Propagation

Given input node features $\mathbf{H}^{(0)} = \mathbf{X}$, the ℓ -th layer of GEGCN updates node representations according to

$$\mathbf{H}^{(\ell+1)} = \sigma(\hat{\mathbf{A}}^* \mathbf{H}^{(\ell)} \mathbf{W}^{(\ell)}), \quad \ell = 0, \dots, L-1.$$

The final node embeddings $\mathbf{H}^{(L)}$ are used for downstream learning tasks.

C Details of Experiments

C.1 Environment

To ensure the reproducibility of our results, we provide the detailed configuration of the experimental environment. All simulations and model training were executed on a Google Colab Pro+ environment with the following specifications:

- **GPU:** A single NVIDIA A100-SXM4 GPU with 40GB of high-bandwidth memory (HBM2). This hardware supports the TensorFloat-32 (TF32) precision format.
- **CPU:** An Intel(R) Xeon(R) CPU running at 2.20GHz (Cascade Lake architecture). The system provides 12 logical cores, supporting the AVX-512 instruction set.
- **Software Stack:** The models were implemented using Python 3.10.12 and PyTorch 2.x. Graph-related operations and message-passing layers were built upon PyTorch Geometric (PyG) 2.4.0. CUDA 12.4 was used as the backend for GPU acceleration.

C.2 Hyperparameter Settings

To ensure the robustness and strong performance of the proposed GEGCN, we conducted automated hyperparameter optimization using Optuna. For each dataset, we performed up to 100 trials over the search space summarized in Table 6. The final configuration for each benchmark was selected based on the highest mean validation accuracy.

Table 6: Hyperparameter Search Space and Optimization Details.

Hyperparameter	Search Range / Values	Distribution
<i>Optimization Parameters</i>		
Learning rate (η)	$[10^{-5}, 10^{-2}]$	Log-uniform
Weight decay (λ)	$[10^{-6}, 10^{-2}]$	Log-uniform
Dropout rate (p)	$[0.01, 0.99]$	Uniform
Hidden dimension (d)	$\{32, 64, 128\}$	Categorical
<i>Curvature & Flow Parameters</i>		
Flow steps (T)	$\{1, 2, \dots, 10\}$	Discrete Uniform
Step size (δ)	$[0.01, 1.0]$	Uniform
Random walk parameter (α)	$\{0, 0.1, \dots, 1\}$	Discrete Uniform
Sinkhorn regularization (ϵ)	0.1	Fixed

C.3 Dataset Statistics

Let $\mathcal{G} = (\mathcal{V}, \mathcal{E})$ be a graph with nodes \mathcal{V} and edges \mathcal{E} . Each node v has a class label $y_v \in \{1, \dots, m\}$. We denote by $d(v)$ the degree of v , that is $d(v) = |\mathcal{N}(v)|$. The homophily index $\mathcal{H}_G \in [0, 1]$, as

proposed by [57], is defined as:

$$\mathcal{H}_G = \frac{1}{|\mathcal{V}|} \sum_{v \in \mathcal{V}} \frac{|\{u \in \mathcal{N}(v) : y_u = y_v\}|}{d(v)}.$$

The detailed homophily index and statistics of the datasets is summarized in Tables 7.

Table 7: Statistics of Datasets.

Dataset	Nodes	Edges	Features	Classes	Homophily ($\mathcal{H}(G)$)
Cora	2,708	5,278	1,433	7	0.81
Citeseer	3,327	4,552	3,703	6	0.74
Pubmed	19,717	44,324	500	3	0.80
Photo	7,650	119,081	745	8	0.83
Coauthor CS	18,333	81,894	6,805	15	0.81
Cornell	183	277	1,703	5	0.12
Texas	183	279	1,703	5	0.06
Wisconsin	251	450	1,703	5	0.17
Chameleon	2,277	31,371	2,326	5	0.23
Actor	7,600	26,659	932	5	0.22
Chameleon-f	890	8,854	2,325	5	0.24
Squirrel-f	2,223	46,998	2,089	5	0.21
Roman-empire	22,662	32,927	300	18	0.05
Amazon-ratings	24,492	93,050	300	5	0.38
Minesweeper	10,000	39,402	7	2	0.68
Questions	48,921	153,540	301	2	0.84

C.4 Pre-computation Details

As shown in Table 8, the discrete Ricci flow is pre-computed offline as a one-time preprocessing step. Although it involves iterative Sinkhorn updates, it introduces no additional latency during model training or inference. The preprocessing cost remains moderate across the benchmark datasets. Even for relatively dense graphs such as Photo, computing $T = 10$ Ricci-flow steps takes about 30 minutes. Moreover, this cost is paid only once and can be reused across different training runs, hyperparameter settings, and random data splits. In practice, this phase can be further accelerated through engineering optimizations, since curvature updates across edges are naturally independent and therefore well suited for parallelization on multi-core CPUs or GPU clusters.

Table 8: Efficiency of offline pre-computation. We report the estimated execution time (in seconds) for computing $T = 10$ steps of Discrete Ricci Flow.

Dataset	Nodes	Edges	Time (s)
Cora	2,708	5,278	34.90
Citeseer	3,327	4,552	2.59
Pubmed	19,717	44,324	851.70
Photo	7,650	119,081	1831.04
Coauthor CS	18,333	81,894	1079.04
Cornell	183	277	4.84
Texas	183	279	3.17
Wisconsin	251	450	5.15
Chameleon	2,277	31,371	745.26
Actor	7,600	26,659	173.01
Chameleon-f	890	8,854	110.74
Squirrel-f	2,223	46,998	2654.67
Roman-empire	22,662	32,927	8.78
Amazon-ratings	24,492	93,050	169.73
Minesweeper	10,000	39,402	77.30
Questions	48,921	153,540	191.13